Journal of Magnetic Resonance 207 (2010) 312–321

Contents lists available at ScienceDirect

Journal of Magnetic Resonance

journal homepage: www.elsevier.com/locate/jmr

IPAP–HSQMBC: Measurement of long-range heteronuclear coupling constants from spin-state selective multiplets

Sergi Gil [a], Juan Félix Espinosa [b], Teodor Parella [a,*]

[a] Servei de Ressonància Magnètica Nuclear, Universitat Autònoma de Barcelona, E-08193-Bellaterra, Barcelona, Spain
[b] Centro de Investigación Lilly S.A., Avda. de la Industria 30, 28108-Alcobendas, Madrid, Spain

ARTICLE INFO

Article history:
Received 1 July 2010
Revised 24 September 2010
Available online 29 September 2010

Keywords:
HSQMBC
Long-range proton-carbon coupling constants
IPAP

ABSTRACT

A new NMR approach is proposed for the measurement of long-range heteronuclear coupling constants ($^nJ_{XH}$, $n > 1$) in natural abundance molecules. Two complementary in-phase (IP) and anti-phase (AP) data are separately recorded from a modified HSQMBC experiment and then added/subtracted to provide spin-state-selective α/β–HSQMBC spectra. The magnitude of $^nJ_{XH}$ can be directly determined by simple analysis of the relative displacement between α- and β-cross-peaks. The robustness of this IPAP–HSQMBC experiment is evaluated experimentally and by simulation using a variety of different conditions. Important aspects such as signal intensity dependence and presence of unwanted cross-talk effects are discussed and examples on the measurement of small proton–carbon ($^nJ_{CH}$) and proton–nitrogen ($^nJ_{NH}$) coupling constants are provided.

1. Introduction

The determination of long-range heteronuclear coupling constants ($^nJ_{XH}$ $n > 1$) is an important parameter in the structural and conformational analysis of small and medium-sized molecules at natural abundance in combination with the more traditional proton-proton coupling constants (J_{HH}) and homonuclear NOE enhancements [1,2]. However, the practical difficulty of finding a simple NMR method for a quantitative and precise measurement of these $^nJ_{XH}$ values has generated the development of two main different strategies. (i) HSQC–TOCSY-type experiments that involve a consecutive magnetization transfer based on $^1J_{XH} + J_{HH}$ for the measurement of $^nJ_{XH}$ only on protonated centers [3–11]. These experiments can afford the J value with precision, simplicity and good sensitivity but the double transfer unfortunately fails for non-protonated heteronuclei or for inefficient homonuclear J_{HH} TOCSY transfer. In these HSQC–TOCSY experiments, the sign and the magnitude can simultaneously be obtained by the analysis of the relative displacement of multiplets in spin-state selective α/β patterns, namely E.COSY, TROSY/anti-TROSY or separate IPAP spectra. (ii) The second approach is based on long-range optimized heteronuclear correlations, such as HMBC [11–16] or long-range HSQC (HSQMBC) [11,17–20] experiments. An important feature of these experiments is that signal intensities strongly depend of the match between the $^nJ_{XH}$ value and the involved inter-pulse evolution delay optimization. In addition, the resulting multiplets usually present complex phase properties due to J_{HH} modulations and with a characteristic anti-phase coupling pattern due to the active $^nJ_{XH}$ coupling that can complicate the multiplet analysis and, therefore, the precise J value extraction. CPMG-INEPT building blocks have been proposed as alternatives to minimize such J_{HH} modulations and post-processing fitting procedures are usually mandatory [11,12,17,18]. A summary of different NMR methods to measure $^nJ_{CH}$ have been reviewed [21,22].

In this work we propose the measurement of the magnitude of $^nJ_{XH}$ from IPAP multiplets in HSQMBC experiments. Our basic approach relies in the acquisition of in-phase (IP) and anti-phase (AP) data in separate HSQMBC experiments. Then, time-domain data are combined (IP ± AP) to provide spin-state-selective α-HSQMBC and β-HSQMBC spectra from which the $^nJ_{XH}$ value can be measured by comparing the relative displacement of a given cross-peak in both spectra. The performance of the method is based on the acquisition of fully complementary IP and AP data in order to avoid excessive cross-talk and undesired differential J_{HH} modulation that could difficult the final multiplet analysis. We demonstrate the usefulness of the proposed NMR method in a variety of conditions and multiplet complexities, by both simulation and practice. Examples on the measurement of small proton-carbon ($^nJ_{CH}$) and proton-nitrogen ($^nJ_{NH}$) coupling constants are provided.

2. Results and discussions

Fig. 1 shows the pulse sequence of the proposed IPAP–HSQMBC experiment. It is based on the original G-BIRD-HSQMBC

* Corresponding author. Fax: +34 93 581 3784.
E-mail address: teodor.parella@uab.cat (T. Parella).

1090-7807/$ - see front matter © 2010 Elsevier Inc. All rights reserved.
doi:10.1016/j.jmr.2010.09.017

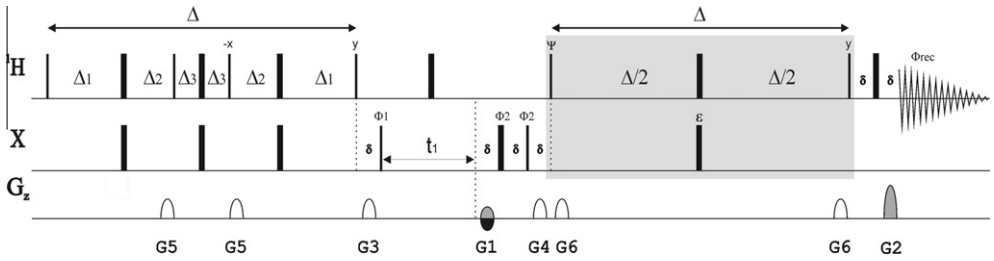

Fig. 1. Pulse sequence of the 2D IPAP–HSQMBC experiment. Thin and thick bars represent 90° and 180° non-selective pulses and are applied along the *x*-axis unless otherwise stated. The basic cycle phase was Φ_1: *x*, −*x*; Φ_2: *x*, *x*, −*x*, −*x*; Φ_{rec}: *x*, −*x*, −*x*, *x*. In-phase (IP) data: $\Psi = y$, ε = on; anti-phase (AP) data: $\Psi = x$, ε = off. The overall Δ delay is optimized to $1/(2 * {}^nJ_{XH})$ ($\Delta = 2\Delta_1 + 2\Delta_2 + 2\Delta_3$, where $\Delta_1 = 1/(8 * {}^nJ_{XH})$, $\Delta_2 = \Delta_1 - \Delta_3$ and $\Delta_3 = 1/(2 * {}^1J_{XH})$). A G-BIRD element is introduced during the first Δ delay in order to minimize direct ${}^1J_{XH}$ responses. G3 and G4 gradients act as *zz*-purge gradient filters, G5 and G6 are used for refocused heteronuclear gradient echo and G1 and G2 are used for coherence selection: G1: 80%, G2: 20.1% for $X = {}^{13}C$ and 8.1 for $X = {}^{15}N$. The sign of the G1 encoding gradient is alternated for echo–antiecho coherence selection.

experiment [16,21] in where an additional refocusing period is added prior to proton acquisition to generate complementary IP and AP data. The G-BIRD element applied during the first Δ delay is used to minimize the intensity of the direct responses. In terms of product operator formalism, no details will be given here for the first part of the sequence because it has already been discussed. The most innovative thing to note is what happens after the variable t_1 period.

Let us consider a ^{1}H nucleus long-range coupled with a heteronuclear *X* spin (usually ^{13}C or ^{15}N), with a small ${}^nJ_{XH}$ coupling value, and also optionally coupled with other ^{1}H by means of J_{HH}. At the end of the variable t_1 period, in where a G1 gradient is applied for coherence selection, single-quantum (SQ) *X* coherences are present in the form:

$$[2H_zX_x\sin_\Omega + 2H_zX_y\cos_\Omega]\sin_X\cos_H \quad (1)$$

where $\sin_\Omega = \sin(\Omega_X t_1)$, $\cos_\Omega = \cos(\Omega_X t_1)$, $\sin_X = \sin(\pi {}^nJ_{XH}\Delta)$, $\cos_X = \cos(\pi {}^nJ_{XH}\Delta)$ and $\cos_H = \cos(\pi \Pi J_{HH}\Delta)$. For simplicity, we will omit these trigonometric factors until the final expressions are analyzed.

Afterwards, the $90°_x(X)$ pulse creates the mixture $2H_zX_x + 2H_zX_z$, and the subsequent purge G4 gradient effectively dephases the first SQ term. In order to generate complementary IP and AP data in terms of relaxation and J_{HH} modulation effects, the highlighted IPAP building block in Fig. 1 is proposed. The IP data, generated using $\Psi = y$, present a main dependence with respect to the $\sin^2(\pi {}^nJ_{XH}\Delta)$ function:

$$2H_zX_z \xrightarrow{90y(I)} 2H_xX_z \xrightarrow{\Delta-180x(I,S)-\Delta} 2H_xX_z\cos_X\cos_H - H_y\sin_X\cos_H$$
$$\xrightarrow{90y(I)} 2H_zX_z \ldots + H_y\cos(\Omega_X t_1)\sin^2(\pi {}^nJ_{XH}\Delta)\cos^2(\pi\Pi J_{HH}\Delta) \quad (2)$$

on the other hand, AP data is obtained using $\Psi = x$ and omitting the central 180° *X* inversion pulse to avoid J_{XH} refocusing. In contrast to IP data, AP data present a main dependence with respect to the $\sin(\pi {}^nJ_{XH}\Delta)$ function:

$$2H_zX_z \xrightarrow{90x(I)} -2H_yX_z \xrightarrow{\Delta-180x(I)-\Delta} 2H_yX_z\cos_H$$
$$\xrightarrow{90y(I)} 2H_yX_z\cos(\Omega_X t_1)\sin(\pi {}^nJ_{XH}\Delta)\cos^2(\pi\Pi J_{HH}\Delta) \quad (3)$$

Finally, a proton spin-echo period incorporating the refocusing G2 gradient selects the desired magnetization before proton acquisition without heteronuclear *X* decoupling. These two IP and AP data are then combined (addition and subtraction) in the time-domain dimension in order to separately yield the spin-state-selective data, which are processed in the conventional way. The resulting α- and β-HSQMBC spectra present excellent phase properties that allow the simple and direct analysis of cross-peak frequency displacement in terms of ${}^nJ_{XH}$ measurement.

To study the performance of our proposal, caffeine (**1**) (Scheme 1) has been chosen as the first test sample to know the behaviour of the IPAP–HSQMBC sequence in simple spin systems without the interference of J_{HH} couplings that could evolve during the evolution Δ delays. Fig. 2 shows the theoretical simulations of the C_5–H_7 cross-peak of **1** (${}^3J_{C5H7} = 2.7$ Hz) in the ^{1}H–^{13}C IPAP–HSQMBC experiment. The intensity modulation of the pure-absorption IP and AP signals (Fig. 2A) clearly illustrates their different $\sin^2$ and sin signal dependence, respectively, as a function of the delay Δ optimization (see Eqs. (2) and (3)). As predicted, maximum signal should be obtained near to $1/2\Delta = 3$ Hz.

The resulting added (IP + AP) and subtracted (IP − AP) multiplets show excellent spin-state selection, as displayed in Fig. 2B. Very importantly, the percentage of cross-talk generated in such addition/subtraction (IP ± AP) procedures due to the non equivalence between IP and AP data is an important issue to assess. It is known that the inefficient suppression of the undesired doublet component in any spin-state selective experiment can affect the accuracy of the *J* measurement. Among the several factors that can severely affect this cross-talk, the mismatch of the Δ delay or the differential relaxation properties between IP and AP components are the most important to consider. Neglecting important relaxation differences in small molecules, the amount the cross-talk in a given multiplet will be proportional to the $\sin^2(\pi {}^nJ_{XH}\Delta) - \sin(\pi {}^nJ_{XH}\Delta)$ factor (Scheme 2) and the percentage of cross-talk with respect to the overall multiplet sensitivity is defined by:

$$\%\text{cross-talk} = [\sin(\pi {}^nJ_{XH}\Delta) - 1]/[\sin(\pi {}^nJ_{XH}\Delta) + 1] \quad (4)$$

Thus, in the case of **1**, whereas maximum sensitivity and a perfect cross-talk matching is observed near 3 Hz, the percentage of cross-talk increases as a function of the $(\sin(\pi {}^nJ_{XH}\Delta) - 1)$ factor (Fig. 2B). In this case, the presence of this undesired cross-talk minimally affects to the measurement via the relative displacement between signals. Fig. 3A shows the theoretical percentage of cross-talk expected for different ${}^nJ_{XH}$ values as a function of the Δ delay optimization in IPAP–HSQMBC experiments. It can be observed that cross-talk is below 20% for a range of ${}^nJ_{XH}$ couplings between 3 and 9 Hz when the experiment is optimized to 6 Hz ($1/2\Delta = 6$ Hz) (Fig. 3B).

Simulated and experimental performances of the above C_5–H_7 cross-peak of **1** in IPAP–HSQMBC experiment differently optimized to $1/2\Delta = 3$, 6 and 9 Hz are compared in Fig. 4. Both theoretical and practical approaches are in very strong agreement and also reproduce maximum AP and IP signal intensities and minimum cross-talk on the experiment optimized to 3 Hz. Despite the decrease of sensitivity, in all cases ${}^nJ_{CH}$ can be accurately measured independent of the Δ optimization and without any scaling factor between IP and AP data. In practice, undesired cross-talk contributions could efficiently be minimized by applying a *k* scaling factor ($k = \sin(\pi {}^nJ_{CH}\Delta)$) in the IP ± k * AP data combination procedure (Fig. 4E).

In order to analyze the important effect of the J_{HH} modulation during the evolution in the Δ delay in the IPAP–HSQMBC

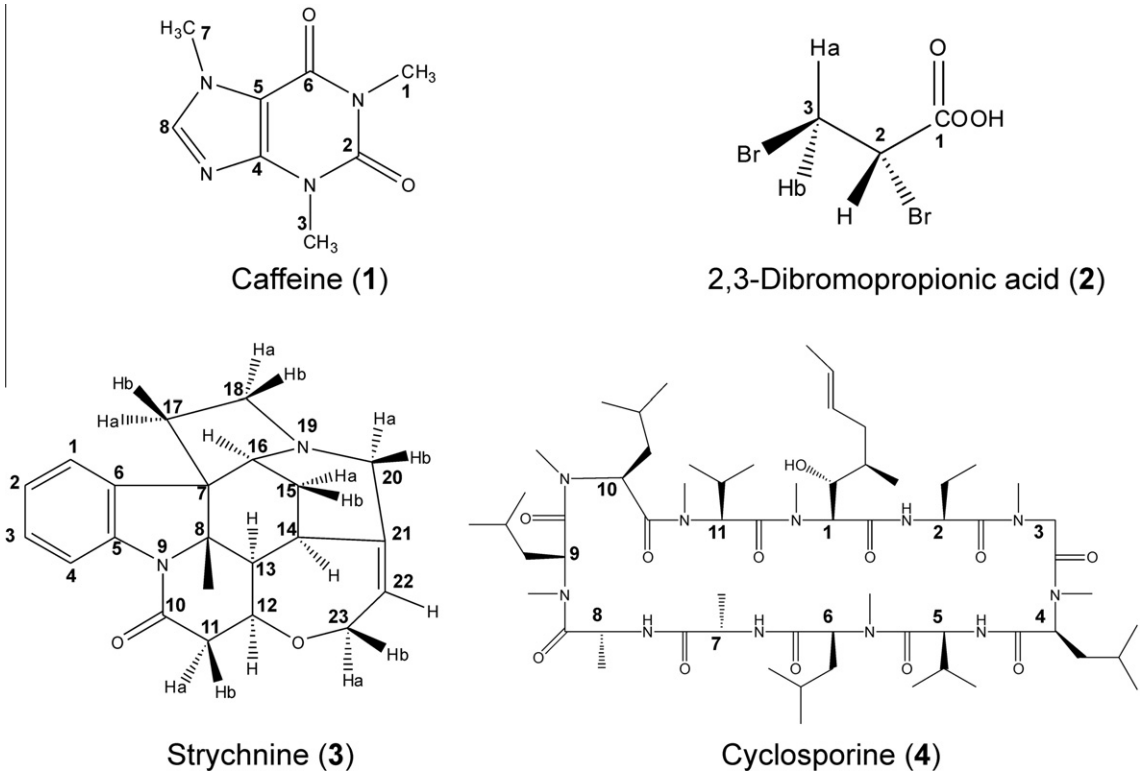

Scheme 1. Structures used in this work.

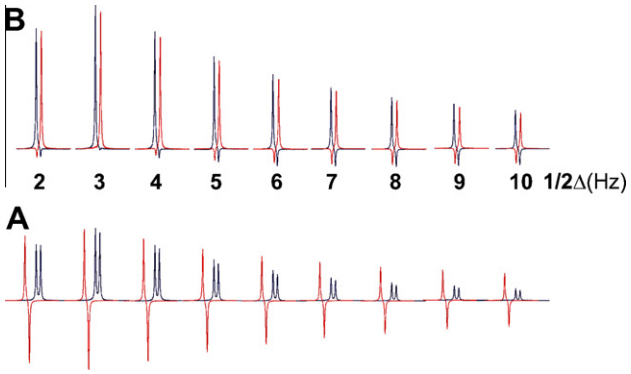

Fig. 2. Simulated cross-peaks for the C_5–H_7 spin-system of **1** ($^3J_{C5H7}$ = 2.7 Hz) in ^{1}H–^{13}C IPAP–HSQMBC optimized to different Δ(=1/($^2J_{XH}$)) values. (A) IP (blue) and AP (red) cross-peaks illustrating the signal intensity dependence as a function of the Δ delay (AP data has been left shifted for a better comparison). (B) Addition (blue) and subtraction (red) of IP and AP data afford spin-state-selective IPAP–HSQMBC multiplets. Note that the presence of cross-talk does not affect to the relative displacement between signals, so a reliable $^nJ_{CH}$ measurement can be done, independent of the Δ optimization. (For interpretation of the references to colour in this figure legend, the reader is referred to the web version of this article.)

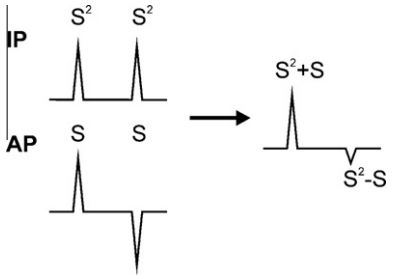

Scheme 2. Signal intensity dependence between the different components in IP (in-phase), AP (anti-phase) and spin-state-selective HSQMBC multiplet patterns.

experiment, both simulated and experimental data obtained from the three different ^{1}H–^{13}C pairs in dibromopropionic acid (DBPA, **2** in Scheme 1) are shown in Fig. 5. Pure-absorption IP (Fig. 5B) and AP (Fig. 5C) data present fully complementary phase properties, so addition and subtraction of their FIDs produces clean α- and β-multiplets (see Fig. 5D). Under the experiment conditions ($1/2\Delta$ = 6 Hz), the percentage of cross-talk expected for the C_3–H_2 ($^2J_{C3H2}$ = −4.0 Hz), C_2–H_{3a} ($^2J_{C2H3a}$ = −4.7 Hz), and C_2–H_{3b} ($^2J_{C2H3b}$ = −3.7 Hz) cross-peaks should be about 7.2%, 2.9% and 9.6%, respectively. It seems clear that the measurement of the $^nJ_{CH}$ coupling value can be made in a very simple manner from the direct analysis of the relative displacement between α and β multiplets in all three cases. To evaluate the importance of the Δ setting, Fig. 6 shows the simulated and experimental results specifically for the C_3–H_2 coupling of **2** in different IPAP–HSQMBC experiments optimized to $1/2\Delta$ = 3, 6 and 9 Hz. In this particular case, the expected percentage of cross-talk should be 7.2%, 7.2% and 21.7%, respectively. Although a considerable loss of signal intensity could be obtained using poor optimized Δ delays, similar $^2J_{C3H2}$ coupling values are measured in all experiments, even with the presence of an important percentage of cross-talk and without application of any k scaling factor. Note that the small deviations in the measurement are within the experimental error of about ±0.2/±0.3 Hz.

To evaluate the practical use of the IPAP–HSQMBC experiment in more complex molecules, Fig. 7B shows some selected α- and β- cross-peaks extracted from the ^{1}H–^{13}C IPAP–HSQMBC spectra of strychnine (**3** in Scheme 1), an alkaloid having a more complex proton spectrum with several types of multiplet patterns and a wide range of $^nJ_{CH}$ values. Examples on both protonated and not

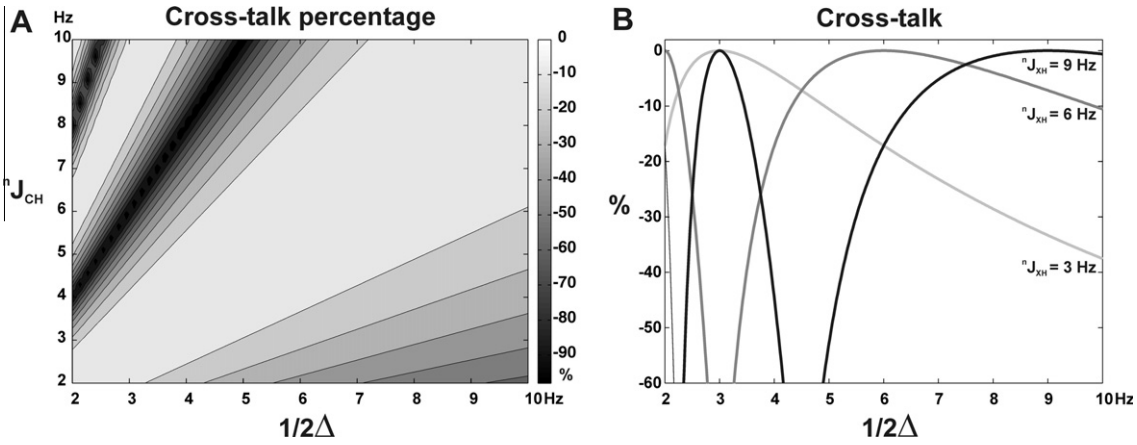

Fig. 3. (A) Theoretical cross-talk dependence (in %) for an isolated ^{1}H–*X* spin system (with a coupling of $^nJ_{XH}$ Hz) as a function of the Δ delay optimization in IPAP–HSQMBC experiments. (B) Percentage of cross-talk expected for couplings of $^nJ_{CH}$ = 3, 6 and 9 Hz.

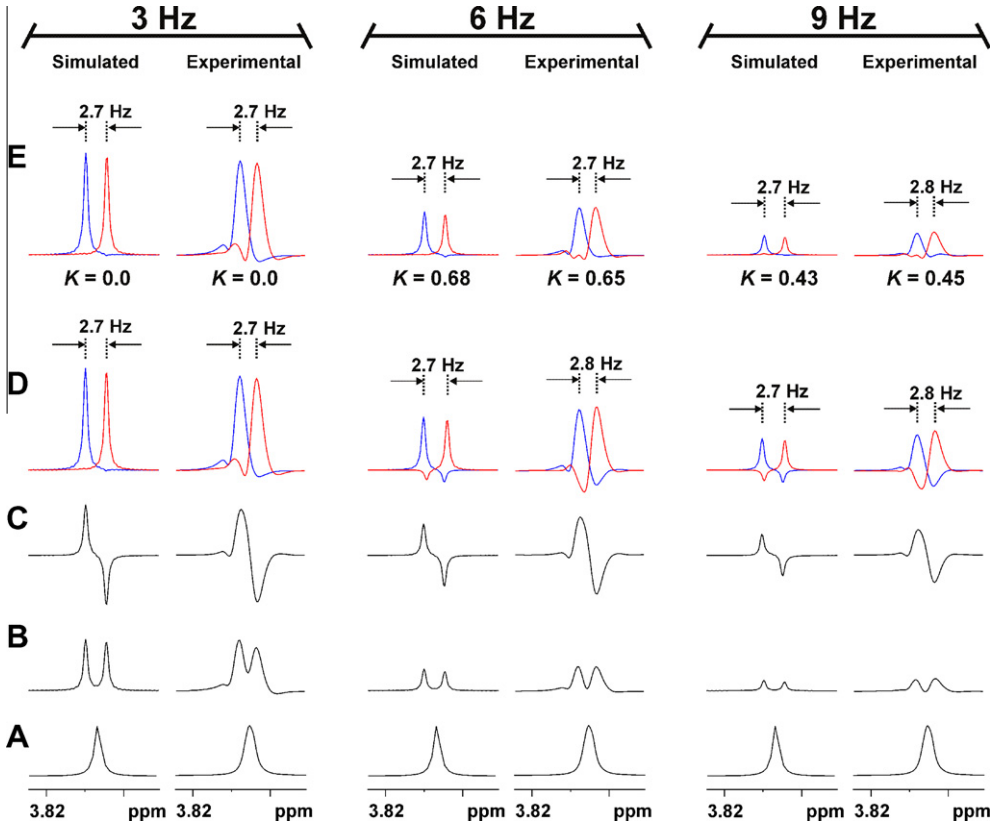

Fig. 4. Simulated (left) and experimental (right) ^{1}H-^{13}C IPAP–HSQMBC cross-peaks for the C_5–H_7 spin-system of **1** ($^3J_{C5H7}$ = 2.7 Hz) with the inter-pulse Δ delays optimized to 3, 6 and 9 Hz. (A) Conventional ^{1}H; (B) IP cross-peaks; (C) AP cross-peaks and (D) IPAP–HSQMBC- α (blue) and β (red) subspectra without scaling factor (AP + IP); (E) IPAP–HSQMBC- α (blue) and β (red) subspectra with a scaling *k* factor according to IP ± *k* ∗ AP. (For interpretation of the references to colour in this figure legend, the reader is referred to the web version of this article.)

protonated carbons demonstrate that the extraction of $^nJ_{CH}$ values can easily be made independent of the cross-peak multiplet complexity and for different levels of undesired cross-talk resulting from a coupling value/delay optimization mismatch. For comparison, AP multiplets obtained from a conventional HSQMBC experiment (Fig. 7C) are also provided in order to show the usual *J* measurement overestimation that can be made by this approach.

Table 1 compares some selected $^nJ_{CH}$ values of **3** determined in this work by the proposed IPAP–HSQMBC experiment and by the IPAP–HSQC–TOCSY experiment [10] with those reported by other methods in early works [9,12,21,23]. In general, our results are in good agreement with them. The observed differences can be attributed to the inherent inaccuracy of each of these methods. In our case, as similar to spin-state selective HSQC–TOCSY type experiments,

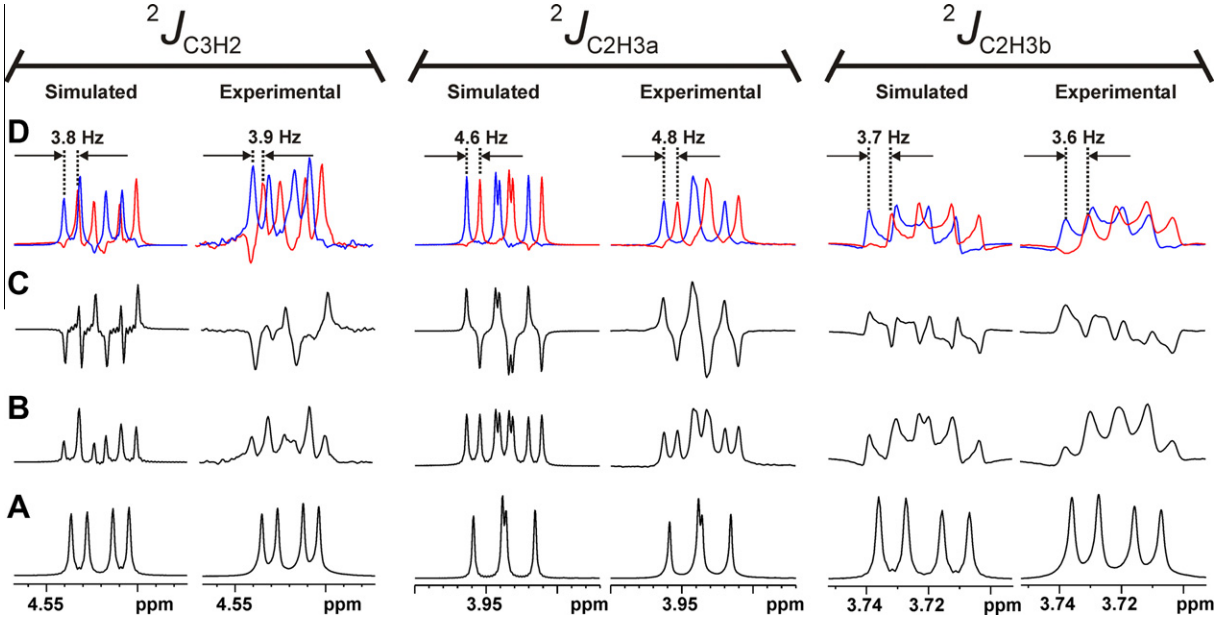

Fig. 5. Simulated (left) and experimental (right) multiplets for the C_3–H_2 ($^2J_{C3H2}$ = −4.0 Hz), C_2–H_{3a} ($^2J_{C2H3a}$ = −4.7 Hz). and C_2–H_{3b} ($^2J_{C2H3b}$ = −3.7 Hz) cross-peaks of **2** in a ^{1}H–^{13}C IPAP–HSQMBC with a Δ delay optimized to 6 Hz. (A) Conventional ^{1}H, (B) IP cross-peak (C) AP cross peak and (D) IPAP–HSQMBC- α (blue) and β (red) multiplets without scaling factor. (For interpretation of the references to colour in this figure legend, the reader is referred to the web version of this article.)

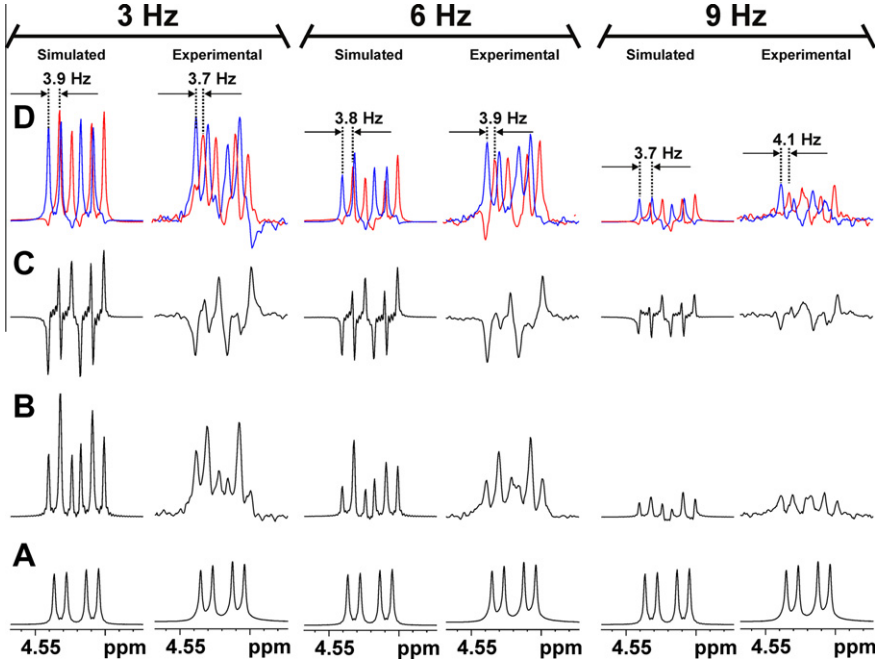

Fig. 6. Simulated 1D (left) and experimental 2D (right) ^{1}H–^{13}C IPAP–HSQMBC C_3H_2 cross-peaks ($^2J_{C3H2}$ = −4.0 Hz) of **2** as a function of the inter-pulse Δ delay optimized to 3, 6 and 9 Hz, respectively. (A) Conventional ^{1}H, (B) IP cross-peak (C) AP cross peak and (D) IPAP–HSQMBC- α (blue) and β (red) subspectra without scaling factor. (For interpretation of the references to colour in this figure legend, the reader is referred to the web version of this article.)

the major inaccuracy can be correlated to the mentioned undesired effects of cross talk that can produce additional separation between the pertinent peaks.

Fig. 8 shows some multiplets extracted from the analog ^{1}H–^{15}N IPAP–HSQMBC spectra of **3**. In this case, the measurement of $^nJ_{NH}$ coupling constants is also performed in a similar straightforward way. Again, the excellent phase properties of the spin-state selective multiplet obtained from the IPAP–HSQMBC pulse sequence facilitates the direct J measurement without any fitting procedure.

It can be accepted that IPAP–HSQC–TOCSY [10] or an equivalent experiment is the method of choice when a very sensitive, simple and precise approach to measure both the sign and the magnitude of any $^nJ_{CH}$ in protonated carbons is required. However, one of the most challenging task should be the precise measurement of small $^nJ_{CH}$ values in non-protonated carbons or nitrogens. In order to evaluate the performance of the proposed experiment for the assignment and the measurement of $^nJ_{CH}$ on carbonyl carbons, several ^{1}H/carbonyl regions of the ^{13}CO-band-selective IPAP–HSQMBC

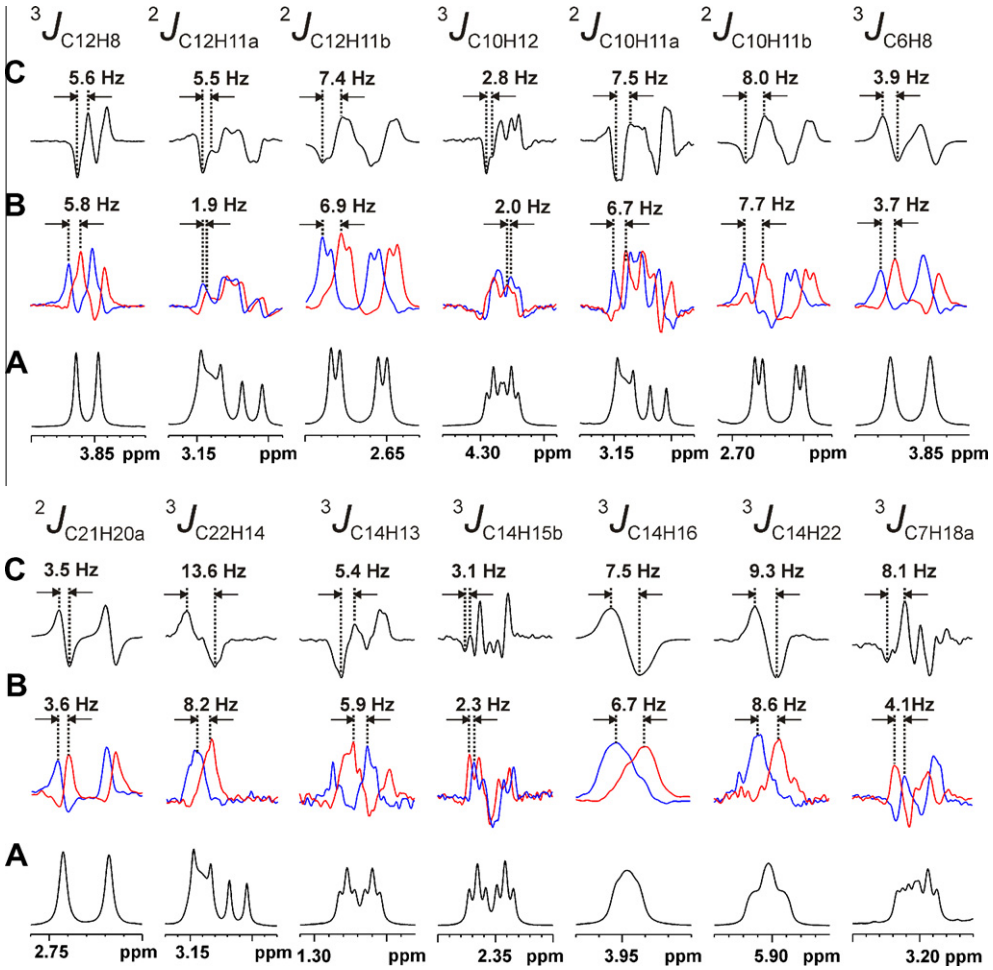

Fig. 7. (A) Conventional ^{1}H, (B) ^{1}H–^{13}C IPAP–HSQMBC- α (blue) and β (red) and (C) ^{1}H–^{13}C AP–HSQMBC selected cross-peaks of strychnine (**3**) recorded with inter-pulse Δ delays optimized to 8 Hz. The measurement of $^{n}J_{CH}$ coupling constants is straightforward for both protonated and non-protonated carbons, due to the excellent phase properties of α- and β-multiplets in (B). Note the overestimation in the measurement made by the direct analysis of the AP multiplet (C). (For interpretation of the references to colour in this figure legend, the reader is referred to the web version of this article.)

spectra of the cyclic undecapeptide cyclosporine (**4** in Scheme 1) are illustrated in Fig. 9. Most of the cross peaks corresponding to the interresidual $^{2}J_{HN\text{-}CO}$, $^{3}J_{Me\text{-}CO}$ and the intra-residue $^{2}J_{HA\text{-}CO}$ can be assigned and measured in a single IPAP–HSQMBC experiment optimized to 8 Hz. On the other hand, the ^{1}H–^{15}N IPAP–HSQMBC spectrum (Fig. 10) clearly illustrates the main advantages of our strategy to measure $^{n}J_{NH}$ coupling constants smaller than 3 Hz. All N-Methyl resonances of **4** are singlets in the proton spectrum and they become doublets in the corresponding HSQMBC experiment due to their $^{2}J_{NH}$ coupling constants with the amide nitrogen center. However, these doublets are not resolved in the IP–HSQMBC experiment due to their small value (Fig. 10B) and the analysis from the anti-phase multiplet obtained in a regular HSQMBC could induce an overestimation in the J measurement (Fig. 10C). The efficiency of the IPAP approach is illustrated in Fig. 10D, where $^{2}J_{NH}$ coupling values around 1.5–2 Hz were efficiently measured for all non-protonated nitrogens in a very simple way.

Two final points must be considered related to the IPAP–HSQMBC experiment. First, the addition of the refocusing delay compared to the original HSQMBC-type experiments introduces a long evolution period into the sequence that undergoes additional signal attenuation due to T 2 relaxation losses. On the other hand, as shown from Eqs. (2) and (3) and also known for related HMBC or long-range optimized HSQC experiments, there is a strong dependence of signal intensity with respect to the passive J_{HH} coupling constants. We have shown that in our approach IP and AP data present similar dependence with respect to the passive J_{HH} and they are efficiently compensated in the addition/subtraction procedure. As an example, Fig. 11 shows the excellent agreement between the theoretical and the experimental signal intensity dependence of the C_2–H_{3a} cross peak of **2** as a function of the Δ optimization in the IPAP–HSQMBC experiment. We can observe that $^{n}J_{CH}$ can be measured with simplicity in all cases when sensitivity is acceptable. However, one inconvenience could be the accidental lack of an expected cross peak due to the unavoidable mismatch Δ setting. In practice, the acquisition of two IPAP–HSQMBC experiments optimized with two different Δ delays could solve such drawback.

In contrast to the IPAP–HSQC–TOCSY experiment, there is no a direct correspondence between the sign of the $^{n}J_{XH}$ coupling and the relative displacement of α/β cross-peaks and therefore it is not possible to determine the sign of $^{n}J_{XH}$ in IPAP–HSQMBC experiments.

3. Methods and materials

Samples of 100 mM of Caffeine in D_2O (**1**), 430 mM of 2,3-dibromopropionic acid in $CDCl_3$ (**2**), 250 mM of Strychnine in $CDCl_3$

Table 1
Comparison of several $^{n}J_{CH}$ constants for strychnine determined in present work and published earlier.

	IPAP–HSQMBC this work	IPAP–HSQC–TOCSY this work	[9]	[12]	[a][21],[b][23]
$^{3}J_{C1H3}$	8.9	+9.3	+8.5	–	–
$^{3}J_{C3H1}$	7.5	+7.2	+7.4	–	–
$^{2}J_{C4H3}$	2.3	+2.5	+2.3	–	–
$^{3}J_{C5H8}$	3.4	–	–	3.2	–
$^{3}J_{C6H8}$	3.9	–	–	3.7	–
$^{3}J_{C7H18a}$	4.5	–	–	4.6	5.2[b]
$^{2}J_{C10H11a}$	6.7	–	–	6.5	6.4[a]
$^{2}J_{C10H11b}$	7.7	–	–	7.9	7.4[a]
$^{2}J_{C11H12}$	2.2	−1.9	−2.1	–	2.5[b]
$^{2}J_{C11H13}$	0.4	−0.5	+0.6	–	–
$^{3}J_{C12H8}$	5.8	+5.6	+5.5	5.5	5.4[a]
$^{2}J_{C12H11a}$	1.9	−2.1	−2.0	2.5	1.7[a]
$^{2}J_{C12H11b}$	6.9	−6.9	−6.9	7.0	7.1[a]
$^{3}J_{C12H23a}$	8.3	–	–	8.6	–
$^{3}J_{C12H23b}$	5.2	–	–	5.6	–
$^{2}J_{C14H13}$	5.5	−4.5	−5.4	4.6	4.7[b]
$^{2}J_{C14H15a}$	1.2	−2.9	−2.7	1.8	3.2[b]
$^{2}J_{C14H15b}$	2.3	−2.6	−3.3	3.2	4.8[a,b]
$^{3}J_{C14H16}$	6.7	+6.4	+6.4	–	6.4[b]
$^{3}J_{C14H20a}$	5.7	+5.4	–	–	–
$^{3}J_{C14H22}$	8.5	+8.6	+6.6	8.5	8.9[b]
$^{3}J_{C18H20b}$	9.3	–	–	9.3	3.6[a], 9.5[b]
$^{3}J_{C18H20a}$	3.6	–	–	3.5	3.6[b]
$^{3}J_{C20H18b}$	7.4	–	–	7.1	7.4[b]
$^{3}J_{C20H22}$	4.6	+5.6	+7.4	4.9	5.7[a],12.5[b]
$^{3}J_{C21H13}$	7.5	–	–	7.8	7.4[a]
$^{2}J_{C21H20a}$	3.6	–	–	2.4	–
$^{3}J_{C22H14}$	8.3	–	–		-
$^{3}J_{C22H20a}$	4.7	+5.0	–	4.5	–
$^{3}J_{C22H20b}$	5.1	+5.5	–	6.1	–
$^{2}J_{C22H23a}$	4.2	−3.8	−3.8	3.8	–
$^{2}J_{C22H23b}$	3.6	−3.4	−3.7	4.0	–

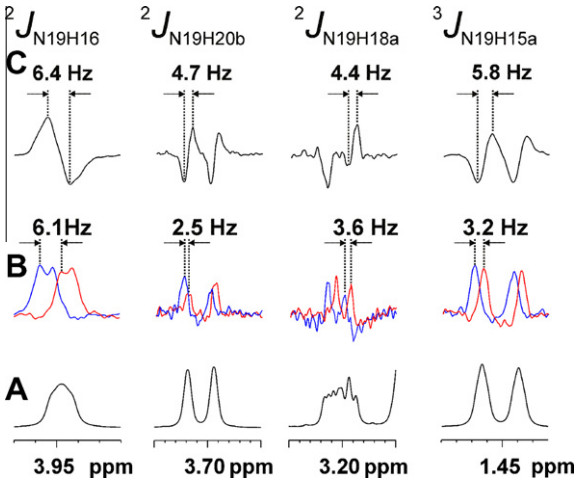

Fig. 8. 1D Slices showing the precise measurement of long-range proton-nitrogen coupling constants of strychnine (**3**) from the $^{1}H–^{15}N$ 2D IPAP–HSQMBC experiment recorded with inter-pulse Δ delays optimized to 7 Hz. (A) Conventional ^{1}H, (B) α (blue) and β (red), and (C) AP selected multiplets. (For interpretation of the references to colour in this figure legend, the reader is referred to the web version of this article.)

(**3**), and 50 mM of cyclosporine in $CDCl_3$ (**4**), were chosen as model samples. NMR experiments have been recorded on a BRUKER 600 Avance II + with a 5-mm broadband TXI inverse probehead incorporating a *z*-gradient coil and on a BRUKER DRX-500 spectrometer equipped with a 3-channel 5-mm TXI inverse probehead incorporating a *z*-gradient coil. All data were acquired and processed with TOPSPIN v2.1 (pulse program is available on request for this platform).

Sine bell shaped gradients of 1 ms duration (δ) are used, followed by a recovery delay of 200 μs. Gradient strengths for the purge *zz*-filters: G3: 33% and G4: 50%; Gradient strengths for coherence pathway are G1: 80%, G2: 20.1% for ^{13}C and 8.1 for ^{15}N. Others gradients are G5: 17% and G6: 5%. Gradients are given as percentage of the absolute gradient strength of 53.5 G/cm. All experiments were acquired and processed using the echo-antiecho protocol.

2D $^{1}H–^{13}C$ IP and AP–HSQMBC experiments on **1** were separately recorded at 600 MHz. The recycle delay was set to 1.5 s, the inter-pulse Δ delay (=$1/2 * {}^{n}J_{CH}$) was optimized to 3, 6 and 9 Hz in different experiments whereas the BIRD delay (Δ_3) was always optimized to 145 Hz (=$1/2 * {}^{1}J_{CH}$). Four scans were accumulated for each one of the 128 t_1 increments and the number of data points in t_2 was set to 8192. Spectral windows in both dimensions were 21,128 (F1) and 3597 (F2) Hz, respectively. The overall acquisition time for each IP and AP data was about 25 min which were added/subtracted in the time-domain without any scaling factor to provide spin-state selective data. Prior to Fourier-transformation of each data, zero filling to 1024 in F1, 16,384 points in F2 and a sine squared function in both dimensions were applied.

2D $^{1}H–^{13}C$ IP and AP–HSQMBC experiments on **2** were separately recorded at 500 MHz using ^{13}C spectral aliasing in the indirect dimension. The recycle delay was set to 1.5 s, the inter-pulse Δ delay (=$1/2 * {}^{n}J_{CH}$) was optimized from 12 Hz to 1 Hz in different experiments whereas the BIRD delay (Δ_3) was always optimized to 160 Hz (=$1/2 * {}^{1}J_{CH}$). Four scans were accumulated for each one of the 32 t_1 increments and the number of data points in t_2 was set to 2048. Spectral windows in both dimensions were 7546 (F1) and 1001 (F2) Hz, respectively. The overall acquisition time for each IP and AP data was about 6 min which were added/subtracted in the time-domain without any scaling factor to provide spin-state selective data. Prior to Fourier-transformation of each data, zero filling to 1024 in F1, 4096 points in F2 and a sine squared function in both dimensions were applied.

2D $^{1}H–^{13}C$ IP and AP–HSQMBC experiments on **3** were separately recorded at 600 MHz. The recycle delay was set to 1.5 s, the inter-pulse Δ delay (=$1/2 * {}^{n}J_{CH}$) was optimized to 8 Hz whereas the BIRD delay (Δ_3) was optimized to 145 Hz (=$1/2 * {}^{1}J_{CH}$). 4 scans were accumulated for each one of the 128 t_1 increments and the number of data points in t_2 was set to 8192. Spectral windows in both dimensions were 24,147 (F1) and 5411 (F2) Hz, respectively. The overall acquisition time for each IP and AP data was about 20 min which were added/subtracted in the time-domain without any scaling factor to provide spin-state selective data. Prior to Fourier-transformation of each data, zero filling to 1024 in F1, 16,384 points in F2 and a sine squared function in both dimensions were applied.

2D $^{1}H–^{15}N$ IP and AP–HSQMBC experiments on **3** were separately recorded at 600 MHz. The recycle delay was set to 1.5 s, the inter-pulse Δ delay (=$1/2 * {}^{n}J_{NH}$) was optimized to 7 Hz whereas the BIRD delay (Δ_3) was optimized to 90 Hz (=$1/2 * {}^{1}J_{NH}$). 32 scans were accumulated for each one of the 64 t_1 increments and the number of data points in t_2 was set to 8192. Spectral windows in both dimensions were 9731 (F1) and 5411 (F2) Hz, respectively. The overall acquisition time for each IP and AP data was about 80 min which were added/subtracted in the time-domain without any scaling factor to provide spin-state selective data. Prior to Fourier-transformation of each data, zero filling to 1024 in F1, 16,384 points in F2 and a sine squared function in both dimensions were applied.

2D $^{1}H–^{13}C$ IP and AP–HSQMBC experiments on **4** were separately recorded at 500 MHz using 10 ms reburp shaped ^{13}C pulses as a band-selective inversion elements in the CO region. The recycle delay was set to 1.5 s, the inter-pulse Δ delay (=$1/2 * {}^{n}J_{CH}$) was optimized to 5 Hz whereas the BIRD delay (Δ_3) was optimized

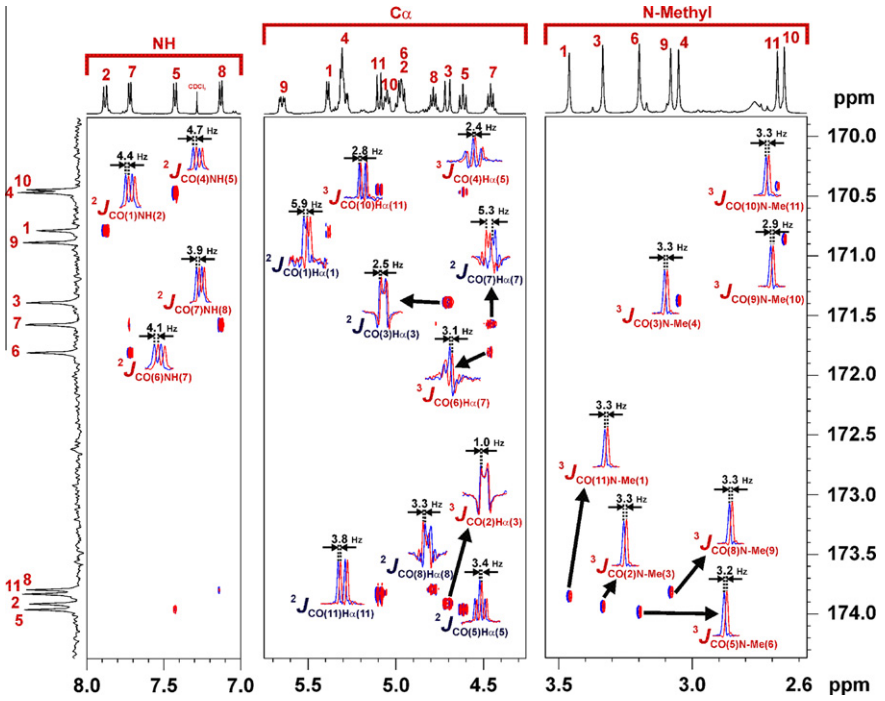

Fig. 9. (A) 2D band-selective $^{1}H–^{13}CO$ IPAP–HSQMBC α (blue) and β (red) subspectra of cyclosporine (**4**) and (B) magnetization transfer scheme encoded with a band-selective ^{13}CO pulse sequence. (For interpretation of the references to colour in this figure legend, the reader is referred to the web version of this article.)

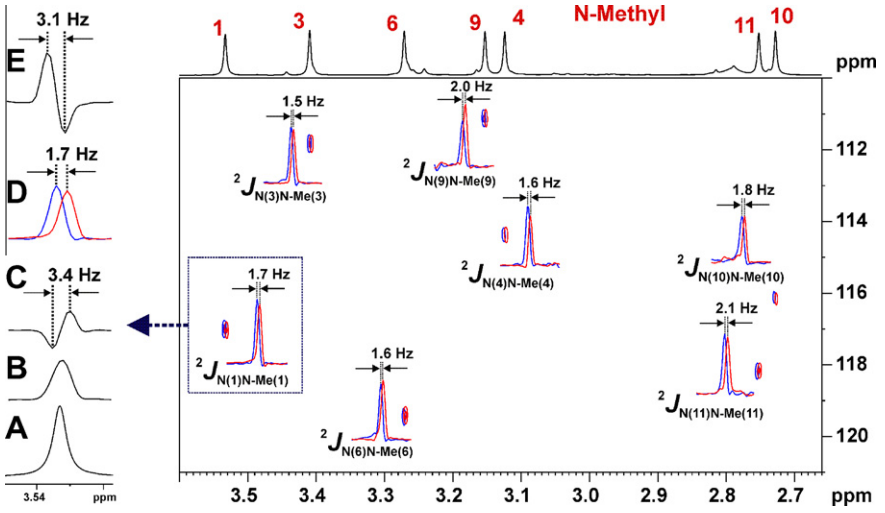

Fig. 10. Measurement of small long-range proton-nitrogen coupling constants from the $^{1}H–^{15}N$ IPAP–HSQMBC spectra of cyclosporine, **4**, with a Δ delay optimized to 3 Hz. 1D slices comparing the conventional (A) ^{1}H and $^{1}H–^{15}N$ IPAP–HSQMBC (B) IP, (C) AP, (D) α (blue) and β (red) cross-peaks, and (E) conventional HSQMBC of N(1)-N-Methyl(1), respectively. Note the overestimation in the measurement of $^{2}J_{N\text{-}Me}$ values from the direct AP multiplet analysis. (For interpretation of the references to colour in this figure legend, the reader is referred to the web version of this article.)

to 135 Hz (=1/2 $*$ $^{1}J_{CH}$). 4 scans were accumulated for each one of the 128 t_1 increments and the number of data points in t_2 was set to 4096. Spectral windows in both dimensions were 1006 (F1) and 4496 (F2) Hz, respectively. The overall acquisition time for each IP and AP data was about 23 min which were added/subtracted in the time-domain without any scaling factor to provide spin-state selective data. Prior to Fourier-transformation of each data, zero filling to 1024 in F1, 8192 points in F2 and a sine squared function in both dimensions were applied.

2D $^{1}H–^{15}N$ IP and AP–HSQMBC experiments on **4** were separately recorded at 600 MHz. The recycle delay was set to 1.5 s, the inter-pulse Δ delay (=1/2 $*$ $^{n}J_{NH}$) was optimized to 3 Hz whereas the BIRD delay (Δ_3) was optimized to 90 Hz (=1/2 $*$ $^{1}J_{NH}$). 8 scans were accumulated for each one of the 64 t_1 increments and the number of data points in t_2 was set to 4096. Spectral windows in both dimensions were 1824 (F1) and 5411 (F2) Hz, respectively. The overall acquisition time for each IP and AP data was about 20 min which were added/subtracted in the time-domain without any scaling factor to provide spin-state selective data. Prior to Fourier-transformation of each data, zero filling to 1024 in F1, 8192 points in F2 and a sine squared function in both dimensions were applied.

Simulations of the 1D version of the IPAP–HSQMBC pulse sequence were made with the NMR-Sim program included in the TOPSPIN software package suite (Bruker Biospin, Germany). Spin system definition used in the simulations: A) Caffeine, **1**: C_5H_7

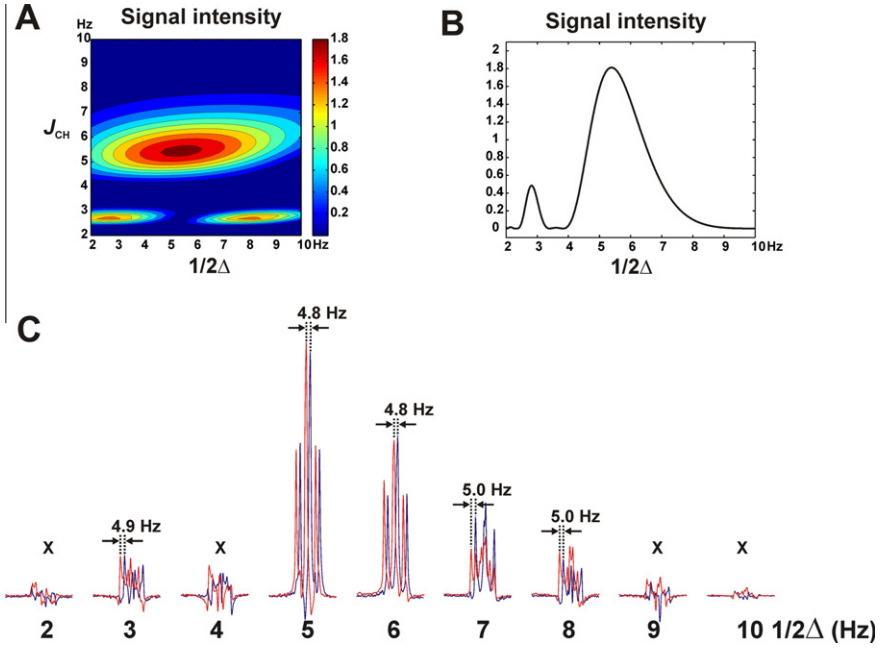

Fig. 11. Signal intensity dependence for the C_2–H_{3a} cross peak of **2** in IPAP–HSQMBC experiment. (A) Theoretical dependence as a function of a range of $^nJ_{CH}$ values and Δ delays, assuming homonuclear coupling constants of $^3J_{H3aH3b}$ = 10.2 Hz, $^3J_{H3aH2}$ = −11.5 Hz; (B) theoretical signal intensity dependence in the case $^2J_{C2H3a}$ = −4.7 Hz; (C) experimental data that is in strong agreement with the theoretical prediction. It can be shown that the measurement of $^nJ_{CH}$ is highly reliable when cross-peak is observed. The sign *X* means that $^nJ_{CH}$ cannot be measured.

spin-system: H_7: 3.8 ppm, C_5: 107.3 ppm, $^3J_{C5H7}$: 2.7 Hz. B) DBPA, **2**: H_2: 4.52 ppm, H_{3a}; 3.94 ppm, H_{3b}: 3.72 ppm, C2: 40.8 ppm, C3: 29.4 ppm, $^3J_{H2H3a}$: 11.5 Hz, $^3J_{H2H3b}$: 4.4 Hz, $^2J_{H3aH3b}$: −10.2 Hz, $^1J_{C3H3}$: 159.4 Hz, $^1J_{C2H2}$: 161.2 Hz, $^2J_{C2H3a}$: −4.7, $^2J_{C2H3b}$: −3.7, $^2J_{C3H2}$: −4.0 Hz.

4. Conclusions

In summary, a modified version of the HSQMBC pulse sequence has been proposed for the easy measurement of long-range heteronuclear coupling constants from spin-state-selective multiplets. The effects of J_{HH} modulation are compensated in the addition/subtraction process of the recorded IP and AP data. Although it should be possible to measure these couplings from individuals IP or AP data, the direct analysis of the α- and β-multiplets allows a more general and easy $^nJ_{XH}$ measurement without any fitting post-processing method. In addition typical errors arising from the existence of poorer resolved multiplets due to broad linewidths or complex *J* patterns, accidental signal cancellation due to anti-phase patterns, or presence of undesired phase distorted multiplets are strongly minimized. The method works well even for the measurement of small coupling values in both protonated and non-protonated carbons and also for other lower sensitive nucleus, such as shown for ^{15}N.

Acknowledgments

Financial support for this research provided by MICINN (projects CTQ2009-08328 and Consolider Ingenio-2010 CSD2007-00006) and by a Bruker-Lilly agreement is gratefully acknowledged. We also thank to the Servei de Ressonància Magnètica Nuclear, Universitat Autònoma de Barcelona, for allocating instrument time to this project.

References

[1] R. Riccio, G. Bifulco, P. Cimino, C. Bassarello, L. Gomez-Paloma, Stereochemical analysis of natural products. Approaches relying on the combination of NMR spectroscopy and computational methods, Pure Appl. Chem. 2–3 (2003) 295–308.
[2] G. Bifulco, P. Dambruoso, L. Gomez-Paloma, R. Riccio, Determination of relative configuration in organic compounds by NMR spectroscopy and computational methods, Chem. Rev. 107 (2007) 3744–3779.
[3] M. Kurz, P. Schmieder, H. Kessler, HETLOC, an efficient method for determining heteronuclear long-range couplings with heteronuclei in natural abundance, Angew. Chem. Int. Edit. 30 (1991) 1329–1331.
[4] W. Kozminski, HECADE: HMQC- and HSQC-Based 2D NMR experiments for accurate and sensitive determination of heteronuclear coupling constants from E.COSY-type cross peaks, J. Magn. Reson. 124 (1997) 383–392.
[5] K.E. Kövér, V.J. Hruby, D. Uhrín, Sensitivity- and gradient-enhanced heteronuclear coupled/decoupled HSQC–TOCSY experiments for measuring long-range heteronuclear coupling constants, J. Magn. Reson. 129 (1997) 125–129.
[6] D. Uhrín, Sensitivity- and gradient-enhanced hetero (ω1) half-filtered TOCSY experiment for measuring long-range heteronuclear coupling constants, J. Magn. Reson. 130 (1998) 155–161.
[7] W. Kozminski, Simplified multiplet pattern HSQC-TOCSY experiment for accurate determination of long-range heteronuclear coupling constants, J. Magn. Reson. 137 (1999) 408–412.
[8] P. Nolis, T. Parella, Spin-edited 2D HSQC–TOCSY experiments for the measurement of homonuclear and heteronuclear coupling constants: application to carbohydrates and peptides, J. Magn. Reson. 176 (2005) 15–26.
[9] M. Misiak, W. Kozminski, Determination of heteronuclear coupling constants from 3D HSQC-TOCSY experiment with optimized random sampling of evolution time space, Magn. Reson. Chem. 47 (2009) 205–209.
[10] P. Nolis, J.F. Espinosa, T. Parella, Optimum spin-state selection for all multiplicities in the acquisition dimension of the HSQC experiment, J. Magn. Reson. 180 (2006) 39–50.
[11] K. Kobzar, B. Luy, Analyses, extensions and comparison of three experimental schemes for measuring (nJCH+DCH)-couplings at natural abundance, J. Magn. Reson. 186 (2007) 131–141.
[12] R.A.E. Edden, J. Keeler, Development of a method for the measurement of long-range ^{13}C–^1H coupling constants from HMBC spectra, J. Magn. Reson. 166 (2004) 53–68.
[13] W. Willker, D. Leibfritz, Determination of heteronuclear long-range H, X coupling constants from gradient-selected HMBC spectra, Magn. Reson. Chem. 33 (1995) 632–638.

[14] K. Furihata, H. Seto, J-Resolved HMBC, a new NMR technique for measuring heteronuclear long-range coupling constants, Tetrahedron Lett. 40 (1999) 6271–6275.
[15] T. Parella, J. Belloc, Spin-state-selective excitation in selective 1D inverse NMR experiments, J. Magn. Reson. 148 (2001) 78–87.
[16] A. Meissner, O.R. Sorensen, Measurement of J(H,H) and long-range J(X,H) coupling constants in small molecules. Broadband XLOC and J-HMBC, Magn. Reson. Chem. 39 (2001) 49–52.
[17] R.T. Williamson, B.L. Márquez, W.H. Gerwick, K.E. Kövér, One- and two-dimensional gradient-selected HSQMBC NMR experiments for the efficient analysis of long-range heteronuclear coupling constants, Magn. Reson. Chem. 38 (2000) 265–273.
[18] K.E. Kover, G. Batta, K. Feher, Accurate measurement of long-range heteronuclear coupling constants from undistorted multiplets of an enhanced CPMG-HSQMBC experiment, J. Magn. Reson. 181 (2006) 89–97.
[19] H. Koskela, I. Kilpeläinen, S. Heikkinen, LR-CAHSQC: an application of a Carr–Purcell–Meiboom–Gill-type sequence to heteronuclear multiple bond correlation spectroscopy, J. Magn. Reson. 164 (2003) 228–232.
[20] V. Krishnamurthy, Excitation-sculptured indirect-detection experiment (EXSIDE) for long-range CH coupling-constant measurement, J. Magn. Reson. A 121 (1996) 33–41.
[21] B.L. Marquez, W.H. Gerwick, R.T. Williamson, Survey of NMR experiments for the determination of ^{n}J (C,H) heteronuclear coupling constants in small molecules, Magn. Reson. Chem. 39 (2001) 499–530.
[22] T. Parella, 2D methods for the measurement of long-range proton-carbon coupling constants, in: G.A. Morris, J.W. Emsley (Eds.), Multidimensional NMR Methods for the Solution State, John Wiley & Sons Ltd, Chichester, UK, 2010, pp. 305–314.
[23] V. Blechta, F. Del Rio-Portilla, R. Freeman, Long-range carbon-proton couplings in strychnine, Magn. Reson. Chem. 32 (1994) 134–137.